

Analysis on the Impact of Taiwan Far-field Earthquakes on the Disaster Avoidance Behavior of People in High-rise Buildings in Large Cities in Southeast China

li dongping (✉ lidongping@zjdz.gov.cn)

Zhejiang Earthquake Agency

Tan Qingquan

Beijing earthquake agency

Yin Jinfei

zhejiang earthquake agency

jian yibo

zhejiang earthquake agency

Research Article

Keywords: mobile data, high-rise buildings, spatial-temporal model, emergency response after earthquake, M6.1 earthquake in Hualien, Taiwan

Posted Date: March 24th, 2022

DOI: <https://doi.org/10.21203/rs.3.rs-998067/v1>

License:   This work is licensed under a Creative Commons Attribution 4.0 International License. [Read Full License](#)

Abstract

Taiwan Province is an earthquake-prone area, and strong earthquakes in Taiwan could affect coastal cities in the mainland. The high-rise buildings in coastal cities often are seriously affected, which can cause social panic. Therefore, it is necessary to study the seismic impact of moderate and strong earthquakes in Taiwan on the mainland coast to accurately analyze the effect on buildings in this area, especially the responses of people in high-rise buildings after the earthquake, and to provide a relatively accurate reference for the evaluation of the timely restoration of social order. This paper uses the 43.29 million mobile phone location records collected after the M6.1 earthquake in Hualien, Taiwan on April 18, 2021, for the bandwidth selection in kernel density estimation in different regions and conducts a quantitative density analysis of 331 buildings using the communication check-in data after the earthquake on different temporal and spatial scales. Through this work, an exponential model of people's responses in high-rise buildings to far-field strong earthquakes in Taiwan is obtained, and the flow pattern of people in regard to disaster avoidance in high-rise buildings after far-field nondestructive earthquakes is summarized. This paper can be a reference for the local government to judge the impact of Taiwan's far-field earthquakes and to make decisions with respect to disaster relief.

Introduction

Taiwan Province is located on the continental edge of the southeast coast of China, close to the convergence boundary of the Eurasian plate and the Philippine Sea plate. The westward push of the Philippine Sea plate and the eastward upthrust of the Eurasian plate form one of the strongest crustal deformation areas. The seismicity in Taiwan is frequent and strong. Since 1900, 42 earthquakes with magnitude (M) ≥ 7 have occurred. Usually, strong earthquakes in Taiwan can affect the southeast coastal areas, including Zhejiang Province and Fujian Province, and some strong earthquakes can even cause certain earthquake damage along the coast (Smith SK. 2006). On September 16, 1994, an earthquake of M7.3 occurred in the southwestern sea area of Taiwan and had a VI-degree impact on the coastal areas of Fujian Province. The M7.2 earthquake in the southwest sea area of Taiwan on December 26, 2006, had a strong impact on the southeastern coast of the mainland, with a maximum impact distance of 1100 km. On March 4, 2010, a M6.7 earthquake struck Kaohsiung, Taiwan and caused a strong shaking in Fuzhou, Xiamen, Quanzhou, and Wenzhou, and the building of Fuzhou Daily shook for approximately 20 seconds. Strong earthquakes in Taiwan can cause long-period ground motion with a displacement of several millimeters in a vast area from the southeast coast to the inland, with a distance of hundreds to thousands of kilometers. With the development of the economy and the acceleration of urbanization, the coastal area is more sensitive to earthquakes, and more attention should be paid to the impact of earthquakes in Taiwan.

China's southeast coastal area has a dense population, developed economy, and high concentration of wealth, includes the most developed economic center in China, is an important international portal in the Asia Pacific region, and has a world-class urban agglomeration and many high-rise and super high-rise buildings (Tomás L et al. 2016). Although a strong earthquake in Taiwan would be far away, the amplification of high-rise buildings leads to strong responses in this region, which could cause great panic. The impact of earthquakes on high-rise buildings is a common concern in this region. This paper

statistically analyzes concrete high-rise buildings in Xiamen, Fuzhou, and Wenzhou by using communication big data, compares the amplification effects of different site conditions, structures, and heights under an earthquake, and obtains the specific human sensitive values and patterns, which provides a technical basis for postearthquake emergency countermeasures (Calka B et al. 2019, Alam M et al. 2009).

Acquisition Of Spatial-temporal Data

At present, internet and communication technology are developing rapidly. Location-related big data, such as smart phone positioning data, social media check-in data, and photos, provide resources for the fast perception of dynamic human changes (Wang et al., 2020). Location check-in data are reported through the application programming interfaces (APIs) of mobile phone systems, and can be used to analyze the geographical locations of users, which is important spatial data. At present, commercially available data mainly include Global Positioning System (GPS) data, Wi-Fi data, and base station signal data used for mobile phone positioning for a large population. Based on the coverage of local mobile terminal devices and the actual population proportion, the real-time population number is obtained through model correction; this is a kind of unclassified statistical data for a large population and does not involve privacy. This work uses GeoHash grids with data accuracy ranging from 5 to 8. In this study, the number of internet terminals ultimately refers to the number of people holding mobile terminals.

Location check-in data are a discrete geographic information system (GIS) point object with spatial coordinates and user attributes. In this study, the discrete check-in data are gridded. The large amount of data and discrete check-in location points are transformed into grid data with spatial continuity and adjacency, which can better reflect the concentrated density of check-in events (Brown V et al. 2001, Nie GZ et al. 2012). A grid with fixed pixel size is constructed and spatially connected, and the key attributes of point check-in data with a spatial inclusion relationship are mapped to the corresponding attributes of the grid. The equations are as follows:

$$D(W) = \sum_{i=1}^n N_{pi} \times \delta_{pi} \cap P_i \subset (\{P\}) \cap G$$

1

$$D(T) = T_k \sum \delta_{p \cap T_k} = \max \left\{ P \sum \delta_{p \cap T_1}, \dots, \sum \delta_{p \cap T_i}, \dots, \sum \delta_{p \cap T_s} \right\}$$

2

where $D(W)$ represents the number of check-ins for grid G ; $D(T)$ represents the area type of grid D ; n represents the number of check-in points in grid D ; N_p represents the total number of check-ins of the i^{th} check-in point in grid D ; δ_{pi} represents the weight of the check-in point; and $\sum \delta_{p, T_i}$ is the sum of the weights of all check-in points of class T_i in grid D . According to Equations (1) and (2), the discrete check-in data are converted into a gridded dataset of check-in frequency, which not only simplifies the discrete point data but also maintains the space-time characteristics and thematic attribute characteristics of check-in data (Sakaki T et al. 2010).

Data Processing Methods

At 22:14 Beijing time on April 18, 2021, a M6.1 earthquake occurred in Hualien County, Taiwan (23.94°N and 121.43°E), with a focal depth of 30 km. The earthquake caused strong shakings throughout Taiwan and obvious shakings in the coastal areas of Fujian Province and could be felt by people in high-rise buildings in Hangzhou, Zhejiang Province. After the earthquake, the wireless internet location data obtained during the earthquake are used to study on the changes in the flow of the public at different scales, the high-resolution real-time mobile terminal location data are used to analyze the spatial-temporal patterns of people gathering and scattering in communities and high-rise buildings after the earthquake, and ideal results are achieved.

2.1 Experimental Area and Data Range

This paper takes the densely populated area affected by the Hualien M6.1 earthquake in Taiwan as the macro-study area. There are 73744 sampling points in 20 periods, and the study area covers urban areas, towns, and villages of 14 cities in southern Zhejiang Province and eastern Fujian Province, including Xiamen, Fuzhou, Putian, Quanzhou, Wenzhou, Lishui, and Taizhou. A total of 43.29011 million people are covered, and the data acquisition accuracy is GeoHash 6. In addition, to analyze the micromovement of people in regard to disaster avoidance in high-rise buildings in large cities, two typical study areas are selected, as shown in Figure 1. The first study area is located in the west of the Siming District, Xiamen city, 360 kilometers from the epicenter, and the data accuracy is GeoHash 8, with 164 sampling points, 176 buildings, and 3032 people. The second study area is located in the commercial and residential area of Longgang city, Wenzhou, 410 km from the epicenter, and the data accuracy is GeoHash 8, with 219 sampling points, 159 buildings, and 3420 people. GeoHash 6 is an approximately 0.6 km × 1.1 km grid, which is more suitable for people flow analysis at the macroscale, and the GeoHash 8 resolution is approximately 20 m × 30 m, which can directly reflect the population flow at the level of a single building and can clearly analyze the phenomenon of people moving from indoors to outdoors. The population information in different periods is extracted. Specifically, the data every 10 minutes from 22:00 on April 18 to 23:40, a total of 10 periods, are extracted, which can comprehensively reflect the dynamic distribution of people after the earthquake. To facilitate comparison, 10 groups of data of the same periods on April 16 and 17 are also obtained.

2.2 Population Distribution using the Kernel Density Method

Because the collected data are summary point data, it is necessary to use a model to simulate the population distribution. Here, the kernel density method is used. Kernel density estimation originates from the first law of geography; that is, everything is related, close things are more closely related, and the closer to the kernel elements are, the greater the density expansion value, which reflects the characteristics of spatial heterogeneity and central intensity attenuation with distance. This method can reveal the detailed characteristics of objects and realize the diffusion of the radiating impact on adjacent locations (Samardjieva E. 2020). It is widely used in research on urban facilities and services, traffic risk assessment, and business congregation spaces. According to the classical population density-distance attenuation relationship, the population density of each grid is simulated. The method can be traced back to the classic Clark model. Through the statistical analysis of more than 20 cities, Clark proposed with convincing evidence that with an increasing distance from the city center to the periphery, the urban

population density tends to decline exponentially; that is, there is a negative exponential relationship between population density and distance (Hadsell R et al. 2006, Haghi, M et al. 2017). The classic Clark model of the spatial distribution of urban population density is shown in Equation (3).

$$D(r) = D_0 e^{-br}$$

3

where r is the distance to the urban center; $D(r)$ is the population density at r from the urban center; D_0 is the scale coefficient, which is theoretically equal to the population density at the urban center; and b is the rate of the distance attenuation effect. Later, two new urban population density models are proposed successively, i.e., the normal density model and negative exponential model. The normal density model is

$$D(r) = D_0 e^{-br^2}$$

4

The negative exponential model is

$$D(r) = kr^{-\alpha}$$

5

where K is the scale coefficient and α is a parameter related to distance. The negative exponential model does not define the population density in the urban center. Most of the population density distribution does not obey the negative exponential model. Studies show that the Clark model is suitable for describing the population density distribution in urban areas, while the negative exponential model is suitable for describing the distribution of population density in urban fringes (Sridharan H et al. 2013, Zhong C et al. 2014).

In this study, the center point of the GeoHash grid is the sample point. In space, people tend to gather near a central point, so the distance from the center is inversely proportional to the population density under normal circumstances (Bossu R et al. 2018). The population distribution in the grid is simulated by calculating the point density attenuation. Kernel density analysis is a suitable method for simulating population distribution. In the calculation of the kernel density, the density does not change greatly with increasing radius. The calculation formula of kernel density estimation is:

$$f(x) = \sum_{i=1}^n \frac{1}{h^2} K \left(\frac{x - x_i}{h} \right)$$

6

where K is the kernel function; h is the search radius (bandwidth), that is, the extension width of the surface near point x in space, which determines the smoothness of the surface of the kernel density; and n is the number of feature points contained by point x in the search bandwidth.

Based on the grid-processed discrete check-in data, exploratory spatial data analysis is used to measure the spatial correlation of check-in data, the spatial structure, and global distribution pattern, and to determine the best mode for hot spot detection and clustering. Cluster analysis is used to identify statistically significant hot spots, cold spots, and spatial outliers. Finally, through the measurement of the geographical and spatial distribution of the clustering analysis results, spatial clustering characteristics of people with statistical significance are obtained, so this is an effective method for detecting the hot spots of population flow and gathering (Hartigan JA et al. 1979, Shaham U et al. 2018).

2.3 Corresponding Relationship between Postearthquake Data Variation and Intensity

In the data analysis, kernel density analysis and rasterization on the point data are conducted, and the density analysis results at 22:10 (before the earthquake) and 22:20 (after the earthquake) on April 18 are used to calculate the grid difference. In the past, elevation data by the digital elevation model (DEM) are often used in grid calculation. Using grid calculation, the difference between the two grid data can be directly obtained. The grid calculation is used to analyze the difference in population density in two periods, and the changes in population before and after the earthquake are obtained (Yu J et al. 2016). In Equation (7), m is the number of people before the earthquake, n is the number of people after the earthquake, s is the gathering degree, s_j is the average daily change within a week, and c is a random value.

$$s = \frac{m - n}{n} - s_j + c$$

7

The area with the largest S value (gathering degree) is the area with the most serious regional impact. In the macroscale calculation, the GeoHash 6 data are used. The calculation results can objectively reflect the people gathering range and degree caused by the earthquake, and then the distribution range around the macroepicenter can be obtained.

Analysis Of The Study Area And Communication Big Data

3.1 Analysis of the Macroscale Variation in Epicenter Communication Big Data

After an earthquake, communication occurs in regard to asking for help or calling relatives and friends. In a nondestructive earthquake, under the premise that the base stations work normally, the overall communication volume and activity in an earthquake-stricken area could certainly continue to increase dramatically, resulting in a phenomenon with many mobile phone turn-ons, sleeps, and activations (Rumelhart DE et al. 1986, Sandholt PE et al. 1998). The closer to the epicenter, the greater the deviation between the trend of the actual mobile phone-based population data and the historical mobile phone-based population data in the affected area is, especially for late night and early morning earthquakes. For example, in the early morning of July 12, 2021, a M5.1 earthquake occurred in Tangshan, Hebei Province. After the earthquake, the number of active mobile internet users in Guye District, Tangshan, which is near the epicenter, increased significantly, while the number of mobile terminals near the macroepicenter increased by 12% within 30 minutes.

First, the intensity distribution of the Hualien earthquake is calculated. Due to the lack of intensity attenuation data in Taiwan, only the theoretical intensity distribution in eastern China is obtained according to the seismic intensity attenuation model, as shown in Figure 1.

$$I_a = 5.253 + 1.398M - 4.164\lg(R + 26) \quad \sigma = 0.632 \quad (8)$$

$$I_b = 2.019 + 1.398M - 2.943\lg(R + 8) \quad \sigma = 0.632 \quad (9)$$

where R is the length of the long axis, I is the intensity, M is the magnitude, and σ is an adjustment parameter.

Figure 2 shows that, macroscopically, the overall changes in human responses are in a discrete state but that the number of active terminals increases significantly in Fuzhou and Putian, which are close to the epicenter, and that the number of active terminals in Ningde and Xiamen, which are far from the epicenter, also increases relatively significantly. In inland areas outside the 3-degree circle, only the number of terminals in urban areas increases to a certain extent. The overall trend shows that in the coastal areas relatively close to the epicenter, the terminal volume increases significantly and changes greatly within cities. In the city, the ground is mostly soil layers and deep bedrock, and there are many high-rise buildings, so a variety of factors interact with each other to amplify the effect of the earthquake. Overall, the change in the terminal density value is obvious and is within the 3-degree circle, but Wenzhou is special, being outside the 3-degree circle, but the number of terminals also increases significantly. The intensity attenuation model used is the point model, and the linear model is more reasonable for earthquakes above $M \geq 6$, which can explain the phenomenon of strong seismic sensation in Wenzhou, as shown in Figure 3 and Table 1.

Table.1 Changes of macro scale overall communication report data

| | Putian | Fuzhou | Ningde | Xiamen | Quanzhou | Wenzhou | Sanming | Nanping |
|---|--------|--------|--------|--------|----------|---------|---------|---------|
| Increased by 10 minutes before the earthquake % % | 3.19 | 3.06 | 2.66 | 2.37 | 2.64 | 2.35 | 1.83 | 1.75 |
| Increase at the same time as the previous day % % | 3.92 | 3.89 | 3.69 | 3.09 | 3.37 | 3.01 | 2.45 | 2.37 |

The time series changes of mobile phone location data in typical areas of Wenzhou and Xiamen are compared, and the curves of the time series changes of the reported location (Figures 4 and 5) are plotted. After the earthquake, the mobile phone location data increases suddenly with the occurrence of the earthquake. In Xiamen, the duration is long, and until 22:50, the curve starts to return to that of the previous day. In Wenzhou, there is a sudden increase, but the duration is short, and there is almost no increase at approximately 22:30. An interesting phenomenon is observed; that is, at approximately 23:30, for these two

cities, the changes in mobile phone location data on the same day are greater than the daily changes, which indicates that some people are still paying attention to the earthquake 1 hour after the earthquake.

3.2 Analysis of the Vertical Spatial Variation in the Population in Building Blocks

Study area 1 (east of the Siming District, Xiamen) and area 2 (north of Longgang city, Wenzhou) containing high-rise buildings are selected (Figures 6 and 7). Because GeoHash 6 data are not accurate enough to reflect the flow of people indoors and outdoors, GeoHash 8 data with a higher accuracy are used. Similarly, Equation 7 is used to calculate the grid density difference in two periods, and the results are shown in Figure 3. People gather in the two study areas. Xiamen is within the 3-degree circle obtained by the theoretical model, while Wenzhou is in an area with an intensity less than 3 degrees according to the model. After the earthquake, some residents move from indoors to outdoor open places, showing disaster avoidance behavior, and the outflow of the population in high-rise buildings is relatively obvious. In the horizontal dimension, many people move out of the core area of the residential area, and crowds gather near the main entrances and exits, the internal roads, and the squares of the community. However, people do not gather at the main traffic lines, especially the city squares and parks relatively far from the residential area, indicating that the residents respond to the earthquake but soon calm down. In the vertical dimension, the population density of high-rise buildings is drastically changed. After a period, most people return indoors, ending their disaster avoidance behavior. The postearthquake disaster avoidance behavior of the population in high-rise buildings is the focus of this study (Akason et al. 2006, Becker et al. 2017).

A high-rise building can be simplified as a vertical cantilever structure. A vertical load mainly produces an axial force in the structure that is roughly linear with the height of the building, and the horizontal load produces a bending moment in the structure (Grasso S et al. 2005). According to the mechanical characteristics, the direction of the vertical load remains unchanged, and only the load increases with increasing building height; the horizontal load can come from many directions, and the force due to lateral deformation increases with increasing height. In high-rise structures, the influence of the horizontal load is much greater than that of vertical load. The impact of the Taiwan earthquake on the southeast coast of the mainland is mainly horizontal displacement produced a far-field earthquake; an additional purpose of this paper is to study the impact of a far-field Taiwan earthquake on the horizontal displacement of high-rise buildings (Freire S. 2010, Erdik M et al. 2011). In the typical areas of Wenzhou and Xiamen, 335 typical buildings with a height of 3-168 m are selected. The change in the population density in buildings below 12 m is not obvious, but obvious changes in population density in buildings between 12 m and 48 m are found. In high-rise buildings with a height of approximately 100 m in Wenzhou and Xiamen, the changes are very close; those in Wenzhou are only slightly smaller. This phenomenon is closely related to the point impact field and linear impact field, as shown in Table 2. In addition, Wenzhou is in an estuarine alluvial plain, with a thick soil layer, so the amplification effect of strong ground motion caused by the soil layer is obvious. However, the buried depth of the soil layer in typical area in Xiamen is shallow, and the ground conditions are good, so the amplification effect is relatively small, as shown in Figures 8 and 9.

Table 2 Comparison of personnel response under buildings of different heights in typical areas of Wenzhou (study area 1)

| | | | | | | | | |
|--------------------------------|------|------|------|------|------|------|------|------|
| Height (m) | 3 | 6 | 9 | 12 | 15 | 18 | 21 | 105 |
| Number of individual buildings | 93 | 35 | 10 | 3 | 9 | 8 | 11 | 2 |
| Number of changes% | 0.21 | 0.43 | 0.61 | 0.79 | 1.13 | 1.45 | 1.76 | 8.44 |

Table 3 Comparison of personnel response under buildings of different heights in typical areas of Xiamen (study area 2)

| | | | | | | | | |
|--------------------------------|------|------|------|-------|-------|------|-------|-------|
| Height (m) | 6 | 9-12 | 18 | 24-36 | 42-48 | 108 | 156 | 168 |
| Number of individual buildings | 8 | 59 | 16 | 41 | 29 | 1 | 2 | 3 |
| Number of changes% | 0.51 | 0.66 | 1.91 | 3.81 | 5.05 | 9.04 | 15.84 | 18.73 |

To study the amplification relationship and pattern of different ground conditions and structures with different heights on ground motion, typical building groups that can fully reflect the regional characteristics are selected for analysis, including 8 high-rise and super high-rise buildings above 100 meters. The analysis results show that for high-rise buildings on hard soil (Xiamen), as the height of the building increases, the sensation of shaking gradually increases; and that for high-rise buildings on soft soil (Wenzhou), the gradual strengthening trend of earthquake sensation is more significant, and the amplification effect of high-rise buildings is more intense (Zhang et al. 2016).

To discuss the macroperformance of the human response in high-rise buildings, the acceleration peak of these 335 high-rise buildings is calculated. According to the relationship between the sense by people on the ground and the peak acceleration of horizontal ground motion in the *Chinese Seismic Intensity Scale*, the following results are obtained: 1) On the soft soil (Wenzhou), the number of people experiencing a strong sensation in 20-meter buildings is approximately 2% more than that on the ground, and the number of people experiencing a strong sensation in 100-meter buildings is approximately 8% more than that on the ground. 2) Due to the lack of data for 150-meter buildings, according to the exponential model, the number of people experiencing a strong sensation is approximately 31% more than that on the ground. 3) On the hard soil (Xiamen), the number of people experiencing a strong sensation in 20-meter buildings is approximately 2% more than that on the ground, the number of people experiencing a strong sensation in 100-meter buildings is approximately 7.5% more than that on the ground, and the number of people experiencing a sensation feeling in 150-meter buildings is approximately 15% more than that on the ground. According to these correlations, when an earthquake occurs, people can reasonably estimate the magnitude of the earthquake by finding the corresponding sensation of people on the ground in the *Chinese Seismic Intensity Scale* to reduce the panic of people in high-rise buildings.

With the support of communication big data, the changes in human response with the floor height on both hard and soft soils are obtained, and enhanced exponential models are obtained.

$$\text{Soft soil } y = 0.5089e^{0.0289x} \quad (10)$$

$$\text{Hard soil } y = 1.0872e^{0.0186x} \quad (11)$$

where Y is the number of people affected and X is the building height. Because of the particularity, this model is applicable only to the impact of Taiwan far-field earthquakes on the southeastern coast of the mainland.

Conclusion

Big data provides an unprecedented social perception means to understand the evolution of natural disasters from a human perspective. This paper quantitatively analyzes the temporal and spatial patterns of people gathering and scattering after an earthquake and studies the postearthquake temporal and spatial changes at different scales, i.e., from urban agglomerations to communities to buildings. New technologies and methods continue to emerge. At present, with the support of high-precision data, the quasi-real-time community level quantitative analysis of postearthquake temporal and spatial changes in population can be achieved, which can provide fine and reliable data at both the macro- and microscales, so that government can provide disaster relief within a few hours after an earthquake. With the support of wireless internet terminal data, this study obtains the spatial-temporal dynamic data of the population after an earthquake at different scales and the quantitative response and disaster avoidance behavior of people in buildings with different heights after an earthquake. Later, after multisource data verification, the data are proved to be close to the actual situation. The actual intensity can be determined by obtaining the human response in high-rise buildings and reduce the panic of people in the high-rise building in regard to the earthquake. Targeted disaster avoidance facilities and escape routes can be designed for high-rise and super high-rise buildings in earthquake prone areas.

The obtained check-in data indicate the number of people that moved in the horizontal direction. Although the data accuracy is high, the lack of direct vertical population changes leads to an inaccurate reflection of the human response in high-rise buildings to the amplified ground motion due to the building height. At present, barometer sensors are used in high-end mobile phones, which can directly reflect the height changes of mobile phone holders. However, the number of sampling points in this study is still small and is not enough to obtain the vertical changes in the overall population. In the future, with increasing numbers of mobile phone sensors, data fusion technology can be used to fuse the number of Wi-Fi signals, the number of people in the horizontal direction, barometer sensors, and other parameters, which can more accurately obtain the changes in people in the vertical direction.

Declarations

Ethical statements

This article is original and not partially published. The article has been written by all participants. The author already knows the journal policy and agree to the copyright transfer.

References

1. Akason JBB, Olafsson S, Sigbjörnsson R (2006) Perception and observation of residential safety during earthquake exposure: A case study. *Saf Sci* 44:919–933

2. Alam M, Mahmoodzadeh A, Pirasteh S (2009) A method for rapid evaluation of masonry buildings against earthquakes. *Int Disaster Adv J* 2(3):15–23
3. Ashbrook D, Starner T (2003) Using gps to learn significant locations and predict movement across multiple users. *Pers Ubiquit Comput* 7(5):275–286
4. Becker JS, Paton D, Johnston DM, Ronan et al (2017) The role of prior experience in informing and motivating earthquake preparedness. *Int J Disaster Risk Reduct* 22:179–193
5. Bossu R, Roussel F, Fallou L, Landès M, Steed R, Mazet-Roux G, Dupont A, Frobert L, Petersen L (2018) LastQuake: from rapid information to global seismic risk reduction. *International Journal of Disaster Risk Reduction* 28:32–42
6. Brown V, Jacquier G, Coulombier D, Balandine S, Belanger F, Legros D (2001) Rapid assessment of population size by area sampling in disaster situations. *Disasters* 25(2):164–171
7. Calka B, Bielecka E (2019) Reliability analysis of LandScan gridded population data. The case study of Poland. *ISPRS Int J Geo Inf* 8(5):222–240
8. Calka B, Costa JND, Bielecka E (2017) Fine scale population density data and its application in risk assessment. *Geomatics Natural Hazards & Risk* 8(1):1–16
9. Dong L, Shan J (2013) A comprehensive review of earthquake-induced building damage detection with remote sensing techniques. *ISPRS J Photogramm Remote Sens* 84:85–99
10. Earle PS, Bowden DC, Guy M (2011) Twitter earthquake detection: earthquake monitoring in a social world. *Ann Geophys* 54(6):708–715
11. Erdik M, Şeşetyan K, Demircioğlu MB, Hancılar U, Zülfikar C (2011) Rapid earthquake loss assessment after damaging earthquakes. *Soil Dyn Earthq Eng* 31:247–266
12. Freire S (2010) Modeling of spatiotemporal distribution of urban population at high resolution—value for risk assessment and emergency management. *Geographic information and cartography for risk and crisis management*. Springer, pp 53–67
13. Grasso S, Maugeri M (2005) Vulnerability of physical environment of the city of Catania using GIS technique. *Adv Earthq Eng* 14:155–175
14. Hadsell R, Chopra S, LeCun Y (2006) Dimensionality reduction by learning an invariant mapping. *IEEE Conference on Computer Vision and Pattern Recognition* 2:1735–1742
15. Haghi M, Ghomi F, Jolai SMT, F (2017) Developing a robust multi-objective model for pre/post disaster times under uncertainty in demand and resource. *J. Clean Prod* 154:188–202
16. Hartigan JA, Wong MA (1979) Algorithm AS 136: A K-Means Clustering Algorithm. *J R Stat Soc Ser C* 28(1):100–108
17. Nie GZ, An JW, Deng Y (2012) Advances in earthquake emergency disaster service. *Seismology & Geology* 34(4):728–791
18. Rumelhart DE, Hinton GE, Williams RJ (1986) Learning representations by back-propagating errors. *Nature* 323:533–536
19. Sadra K, Masakatsu M, Hassanzadeh R, Amiraslanzadeh R, Kamel B (2014) A GIS-based seismic hazard, building vulnerability and human loss assessment for the earthquake scenario in Tabriz. *Soil*

20. Sakaki T, Okazaki M, Matsuo Y (2010) Earthquake Shakes Twitter Users: Real-Time Event Detection by Social Sensors. Proc., Proc International World Wide Web Conference
21. Samardjieva E (2002) Estimation of the expected number of casualties caused by strong earthquakes. Bull Seismol Soc Am 92(6):2310–2322
22. Sandholt PE, Farrugia CJ, Moen J et al (1998) A classification of dayside auroral forms and activities as a function of interplanetary magnetic field orientation. J Geophys Res Space Physics 103(A10):23325–23345
23. Shaham U, Stanton K, Li H (2018) Spectralnet: Spectral clustering using deep neural networks. In International Conference on Learning Representations(ICLR2018), Vancouver, Canada, 1–20
24. Smith SK (1996) Demography of disaster: population estimates after hurricane Andrew. Popul Res Policy Rev 15(5–6):459–477
25. Sridharan H, Qiu F (2013) A spatially disaggregated areal interpolation model using light detection and ranging-derived building volumes. Geogr Anal 45(3):238–258
26. Tomás L, Fonseca L, Almeida C, Leonardi F, Pereira M (2016) Urban population estimation based on residential buildings volume using IKONOS-2 images and lidar data. Int J Remote Sens 37(sup1):1–28
27. Wang Y, Taylor JE (2018) Coupling sentiment and human mobility in natural disasters: a twitter-based study of the 2014 SouthNapa. earthquake Nat Hazards 92(2):907–925
28. Yu J, Wen JH (2016) Multi-criteria satisfaction assessment of the spatial distribution of urban emergency shelters based on high-precision population estimation. International Journal of Disaster Risk Science 7(4):413–429
29. Zhang XB, Kelly S, Ahmad K, lee (2016) The slandail monitor: real-time processing and visualisation of social media data for emergency management. In:Proceedings of 2016 11th International Conference on Availability, Reliability and Security. IEEE, New York, pp. 786-791
30. Zhong C, Arisona SM, Huang X, Batty M, Schmitt G (2014) Detecting the dynamics of urban structure through spatial network analysis. Int J Geograph Inf Sci 28(11):2178–2199

Figures

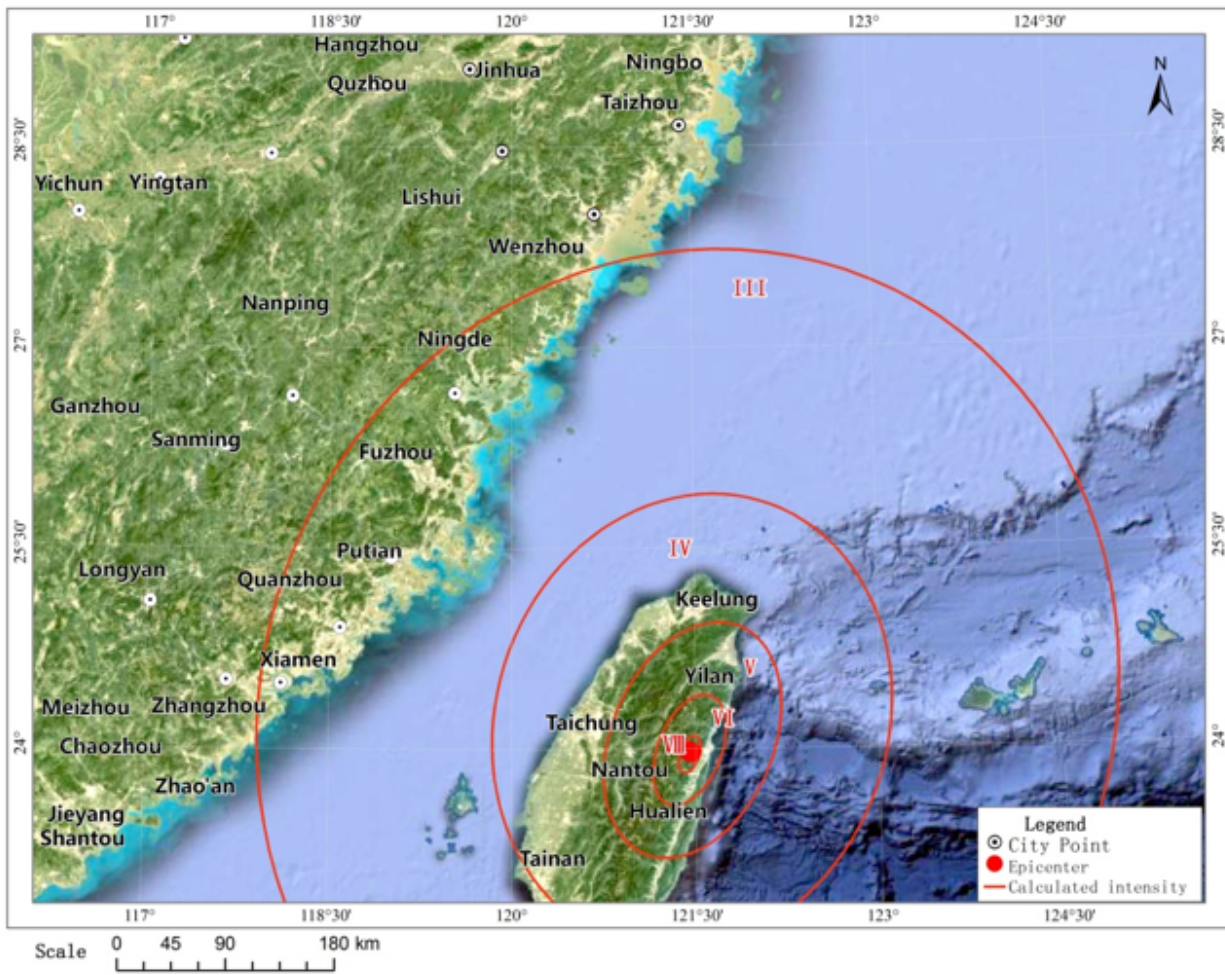


Figure 1

Distribution of the theoretical influence field of the Hualien M6.1 earthquake

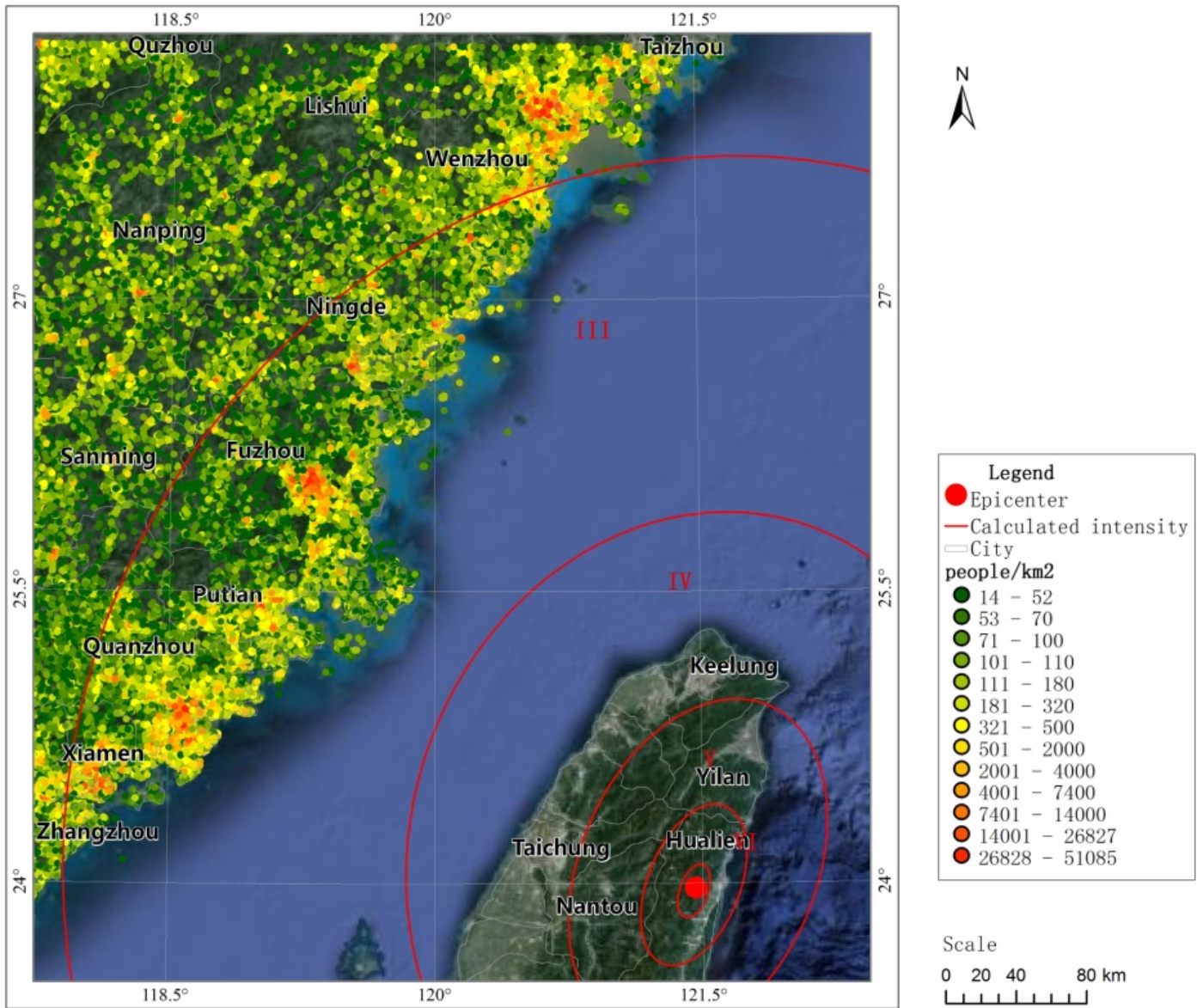


Figure 2

Distribution of the communication big data of the Hualien M6.1 earthquake

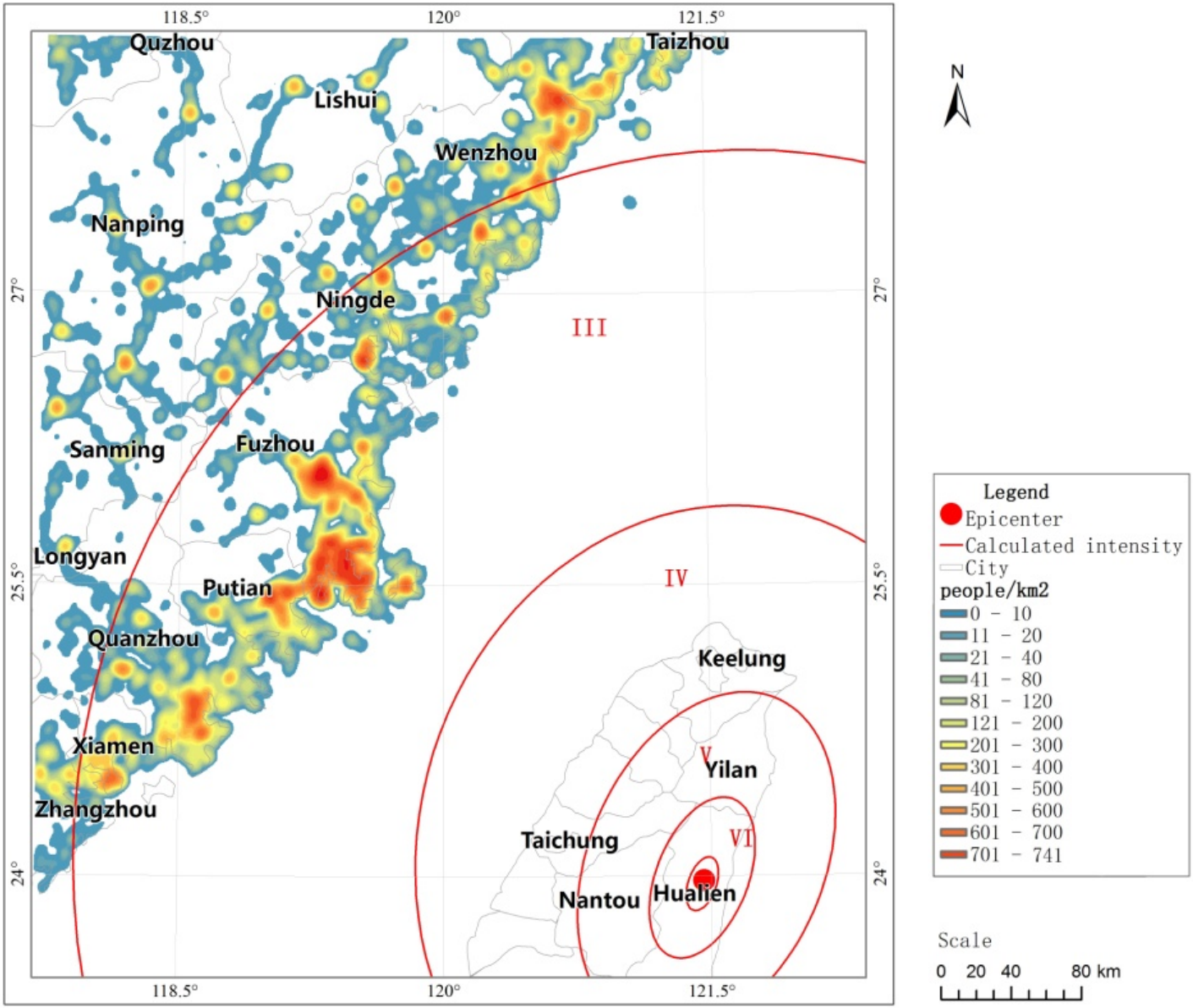


Figure 3

Distribution of the communication impact degree of the Hualien M6.1 earthquake

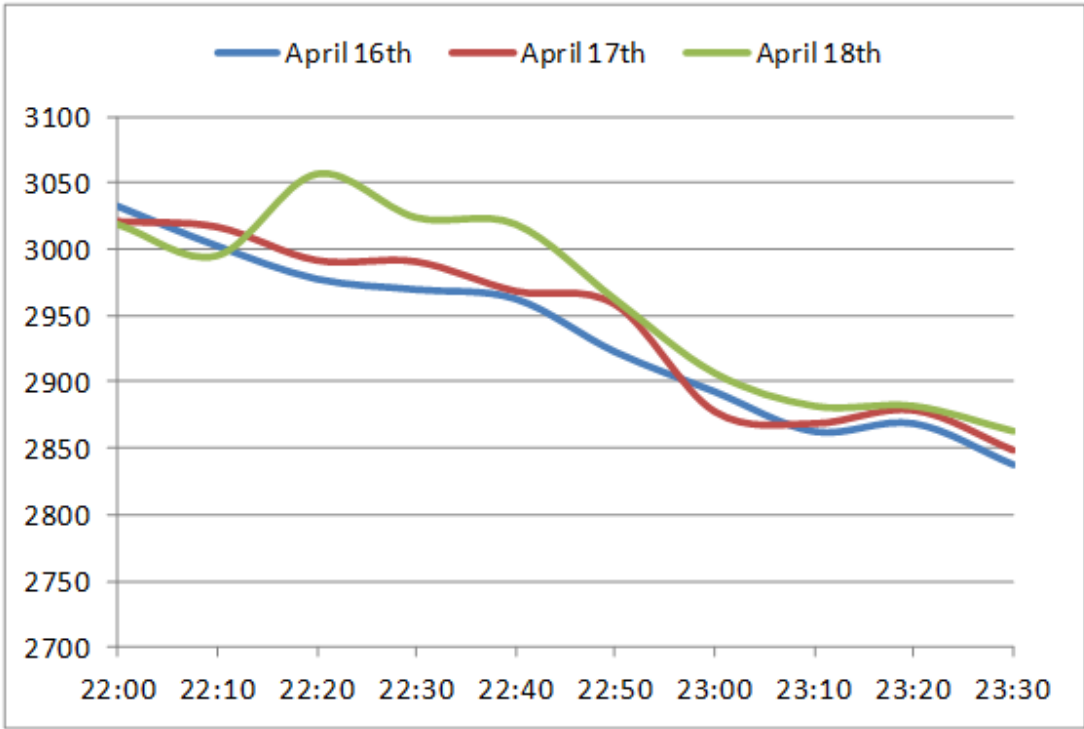


Figure 4

temporal changes of location data reported by mobile phones in typical areas of Xiamen (study area 2)

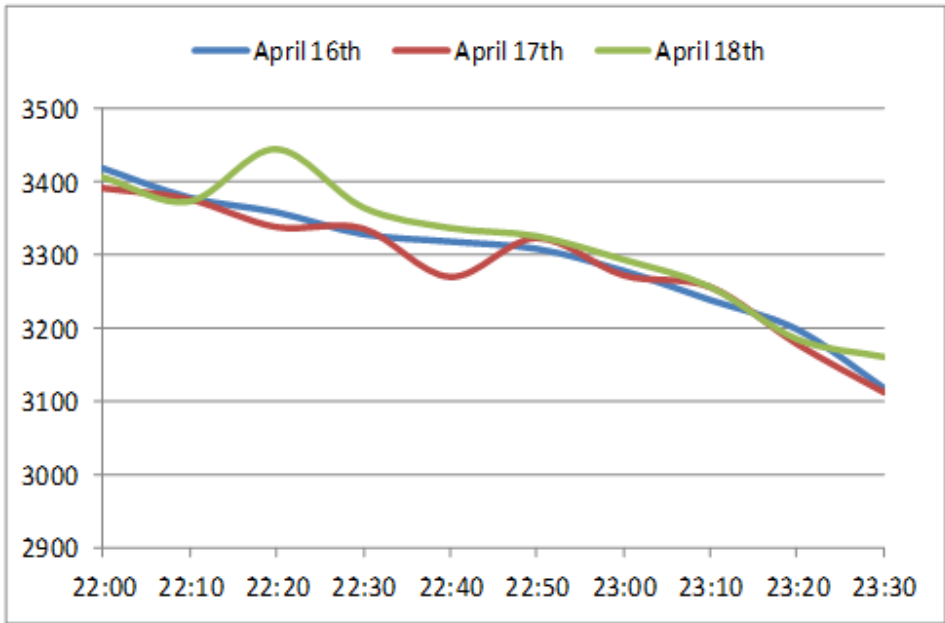


Figure 5

temporal changes of location data reported by mobile phones in typical areas of Wenzhou (study area 1)



Figure 6

Schematic diagram of the location around Wenzhou Kangxin building in study area 1



Figure 7

Schematic diagram of the location around Xiamen Pengyuan building in study area 2

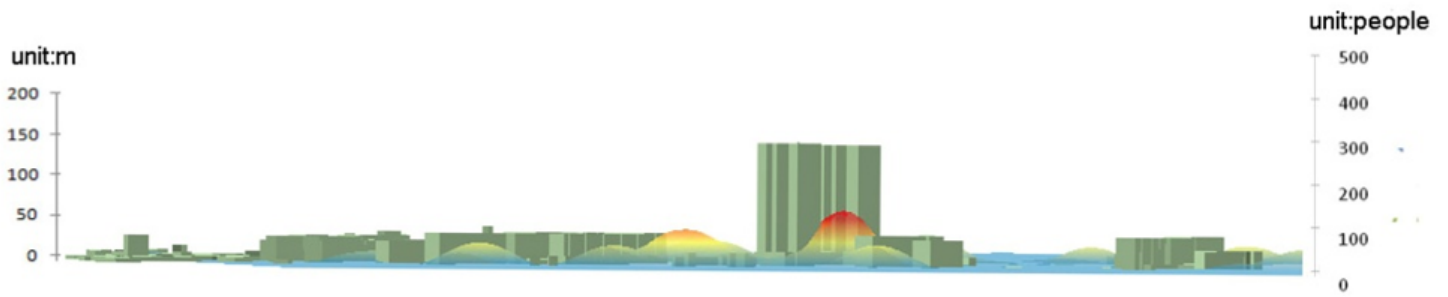


Figure 8

changes of mobile phone location in different buildings in Wenzhou (study area 1)

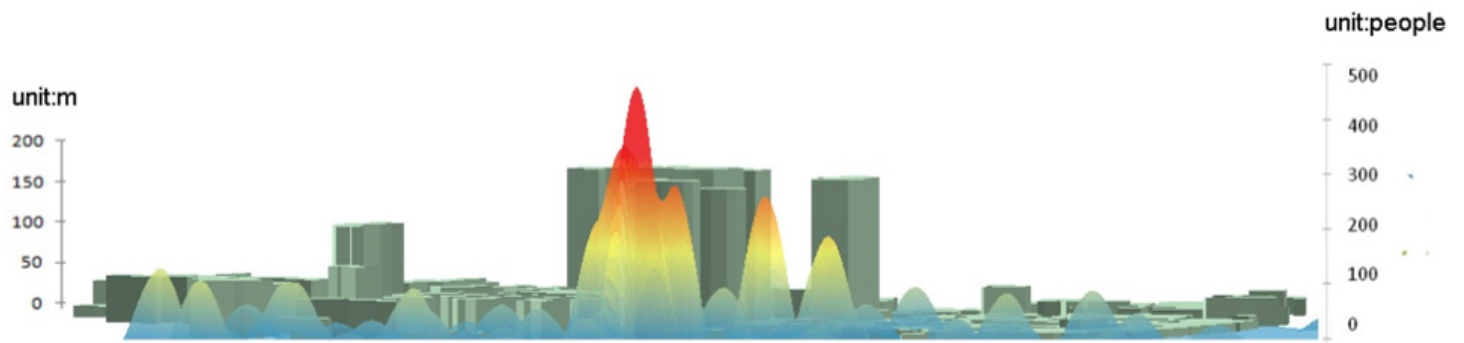


Figure 9

changes of mobile phone location in different buildings in Xiamen (study area 2)

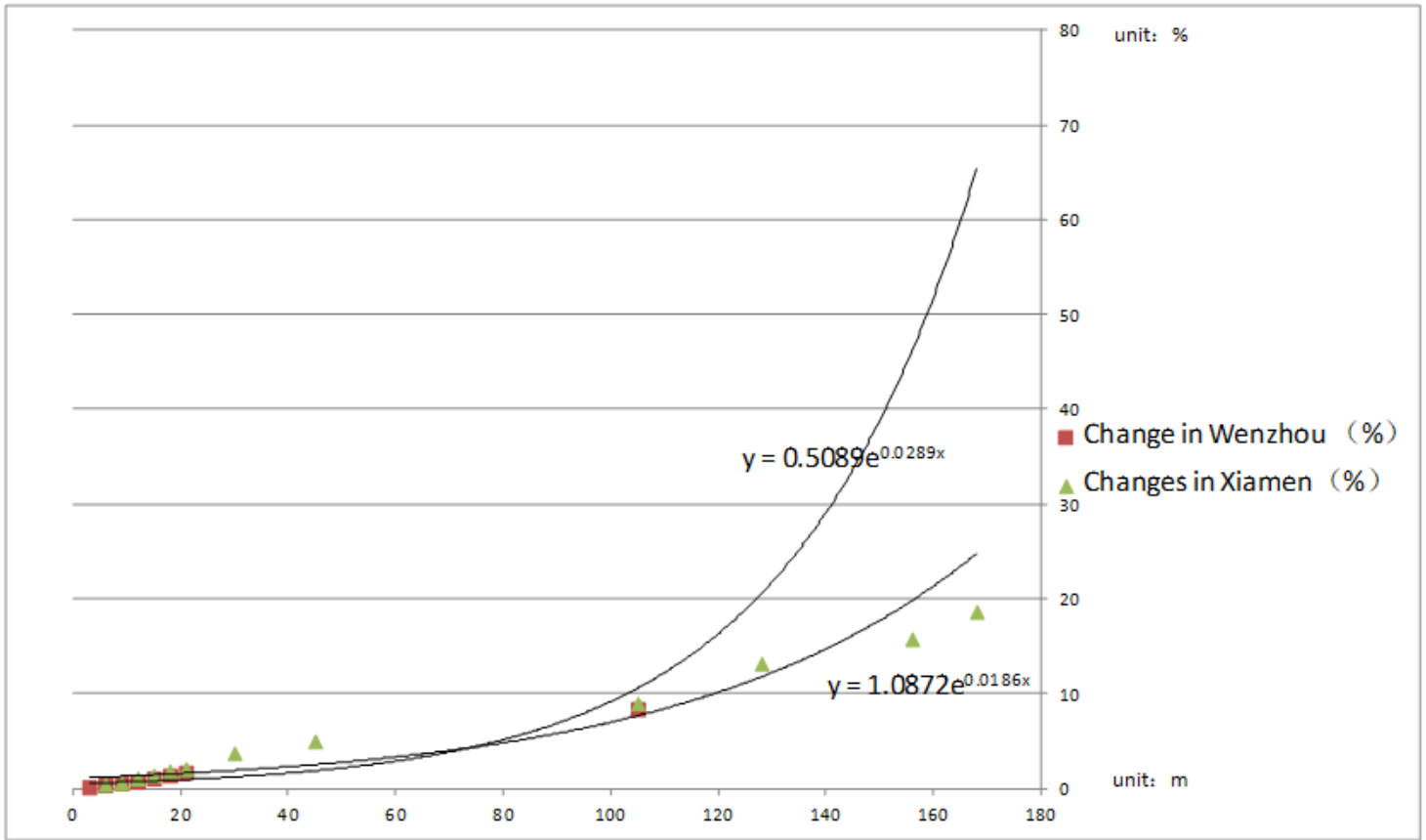


Figure 10

Exponential relationship between human response and floor height